Flexural capacity of negative moment region NSM-CFRP strengthened RC T-beam under high loading rate: An analytical prediction

Laurencius Nugroho[1], *Yanuar* Haryanto[2,3*], *Hsuan-Teh* Hu[1,4], *Fu-Pei* Hsiao[1,3], *Ay* Lie Han[5], *Arnie* Widyaningrum[2], and *Hari* Prasetijo[6]

[1]Department of Civil Engineering, National Cheng Kung University, Tainan, Taiwan
[2]Department of Civil Engineering, Universitas Jenderal Soedirman, Purbalingga, Indonesia
[3]National Center for Research on Earthquake Engineering, Taipei, Taiwan
[4]Department of Civil and Disaster Prevention Engineering, National United University, Miaoli, Taiwan
[5]Department of Civil Engineering, Universitas Diponegoro, Semarang, Indonesia
[6]Department of Electrical Engineering, Universitas Jenderal Soedirman, Purbalingga, Indonesia

Abstract. In the design phase of strengthening a reinforced concrete (RC) beam, it is necessary to determine its capacity. Response-2000 software offers efficient analysis for determining the capacity of a beam, including its flexural capacity. The aim of this study is to assess the predictive accuracy of Response-2000 software in determining the flexural capacity of the negative moment region of NSM-FRP strengthened RC T-beams under high loading rates. The validation of the static material model was initially conducted and then several combinations of established empirical formulations were utilized to express the corresponding dynamic properties of relevant materials. The findings of the study suggest that the compressive and tensile strength of concrete have a significant impact on the flexural capacity of the strengthened beams. Furthermore, empirical evidence supports the idea that Response-2000 possesses the capability to effectively predict the flexural capacity, utilizing a rate-dependent material approach.

1 Introduction

Existing reinforced concrete (RC) structures must be updated or strengthened to provide an adequate safety level over their lifetime. The reasons for this include: non-standard construction work, additional service loads, low material qualities, updating of old codes, and natural disasters [1-6]. Fiber-reinforced polymer (FRP) has gained extensive interest and has become widely used in practical applications because of its high tensile strength, it is lightweight, and has good resistance to corrosion and fatigue [7-9]. The application of FRP using the near-surface-mounted (NSM) technique provides better bond performance between FRP strips or bars and concrete than the conventional externally bonded (EB) technique [10-12]. By embedding FRP strips or bars into grooves on concrete covers, the NSM-FRP effectively increases FRP strain at debonding, due to the confinement of debonding failure by the surrounding concrete cover, which results in increased load-bearing capacity [13, 14].

The NSM-FRP strengthening technique has primarily been used for enhancing the flexural capacity of RC beams [11, 15-19] by inserting the FRP rods or strips into the tension surface. In the context of the monotonic load, Haryanto et al. [20] showed that the NSM-FRP rod on a beam successfully reduces the flexural cracks.

Furthermore, the first crack, yield, and ultimate strength were found to be increased in comparison with an un-strengthened specimen. In addition, Zhang et al. [21] discovered that, by having a more uniform distribution, the potential for the FRP end concrete cover separation may be prolonged, and the ultimate load of the strengthened beams increased as the bond length of the NSM-FRP increased. Moreover, the effect of FRP material on the strengthened beam was observed. For instance, the NSM-carbon FRP (CFRP) created higher flexural strength and stiffness on beams compared to specimens strengthened with glass FRP (GFRP) [22].

The findings from several studies serve as a foundation for guidelines to strengthen beams using NSM-FRP. For instance, the ACI 440-2R [23] guideline highlights several parameters for strengthening a flexural member to obtain its effectiveness, development length, embedment depth, and stress limit. Moreover, ACI 440-2R provides the sectional analysis procedure to determine ultimate strength based on the bending moment capacity involving an FRP strip or rod. The approach taken by this guide follows the philosophy of ACI 318 [24]. During the strengthening design, this approach could be useful as a preliminary illustration of the bending capacity that will be obtained from several reinforcement schemes. In addition, the advanced method using finite element

* Corresponding author: yanuar.haryanto@unsoed.ac.id

software would be expensive, complex, and too long for rapid estimation.

Bentz [25] introduced Response-2000 (R2K) as a cross-sectional analysis software based on Modified Compression Field Theory (MCFT) [26]. This software package can predict the shear strength and full load-deformation response of an RC beam under the influence of shear, moments, and axial load. The Response-2000 software provides a user-friendly interface and quick analysis for any plane geometry and material of an RC beam. Moreover, the current version has user material features for concrete. Metwally [27] and Suryanto et al. [28] showed that the Response-2000 program is able to accurately estimate the shear strength of reinforced and pre-stressed concrete beams. In addition, the accuracy of the result was better with standard provisions. However, Response-2000 is limited to the case of beams that have cantilever and simply supported boundary conditions. Furthermore, the load-displacement response from Response-2000 exhibits an initial linear-static response, followed by a nonlinear transition response and a sudden decline after peak load; it is not well reproduced after peak load, which, consequently, tends to underestimate ductility [29-31]. Nonetheless, the predicted peak load was sufficiently close to the experimental results. Therefore, if the consideration is to assess the load capacity of a beam, this is still acceptable. This assessment was utilized by Haryanto et al. [32], who conducted a design-oriented parametric study about a strengthened RC beam using NSM-FRP rods. The effect of FRP rod diameter, compressive strength ratio of steel reinforcement, and different types of NSM-FRP rods were observed in terms of load capacity.

This study examines the validity of the Response-2000 program in obtaining the ultimate load of a beam strengthened with NSM-FRP rods under high loading rates. The characteristics of an RC beam are affected by the loading rate, which is related to loading rate sensitivity on material properties. The literature demonstrates that concrete can display increased failure stress under both compression and tensile stresses under dynamic loading circumstances. Similarly, it has been shown that an increase in strain rate leads to an increase in both the yield strength and ultimate strength of reinforcing steel. These rate-dependent behaviors are formulated based on experimental results to predict the real behavior of a structure under extreme loads. Finally, several combinations of formulation are utilized to obtain the dynamic properties of concrete and steel on an RC beam.

2 Development of analytical model

2.1 Description of experimental program

The analytical investigation was validated by comparing it with experimental results, as presented in the study conducted by Haryanto et al. [20]. Three RC T-beams were subjected to reverse cyclic loading. As shown in Figure 1, the total length of a beam was designed to be 2600 mm while the total height of the T-section was 300 mm, with a web-width of 150 mm, flange-width of 600 mm, and flange-depth of 120 mm. In addition, two steel rebars with a diameter of 16 mm were used as reinforcement in the tension and compression zones. Meanwhile, the beam flange had four longitudinal plain steel bars with a diameter of 10 mm. The 10 mm-diameter stirrups were placed at a distance of 175 mm in the flange and web of the beam. The two beams were strengthened by utilizing two 8-mm-diameter NSM-CFRP rods on a flange beam, representing the negative moment region on the actual structure. The grooves were created on a concrete cover and filled with rods and epoxy as a filling material. One strengthened beam applied fully embedded CFRP rods, according to a specific code (BF beam), while another only embedded half of the rod's section (BH beam). The section detail for the strengthened beam is shown in Figures 1(a) and 1(b).

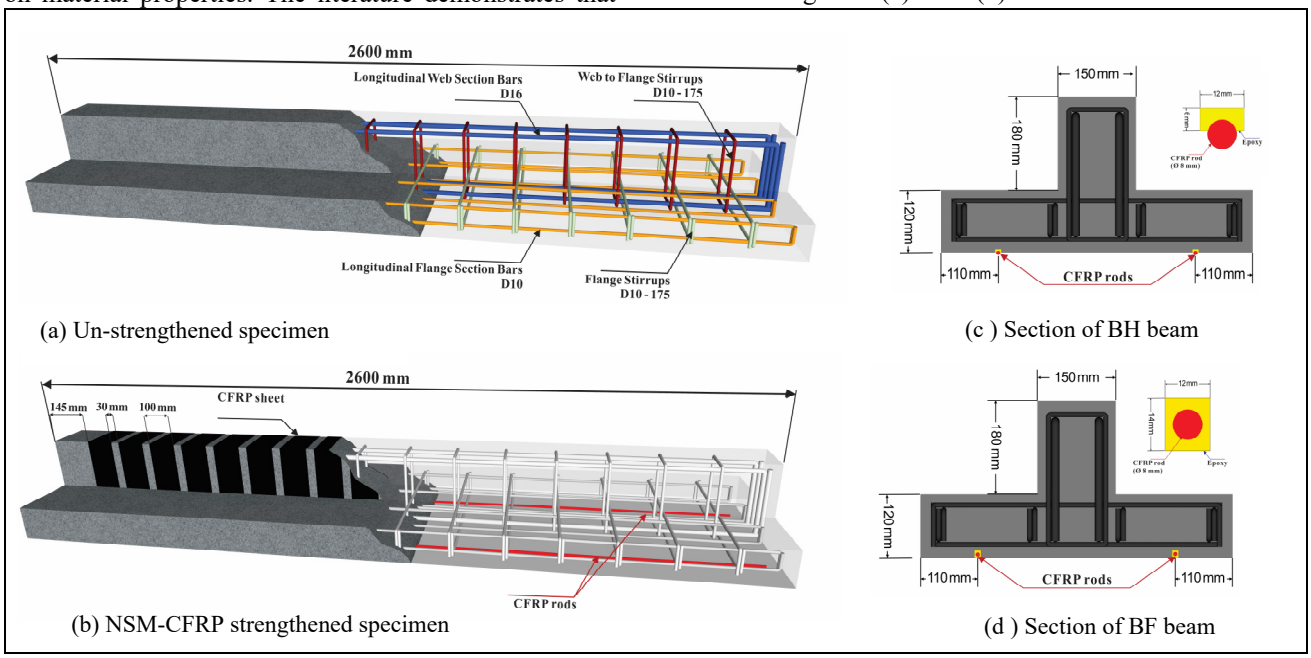

Fig. 1. Specimen details.

Moreover, shear strengthening was outfitted with a 100 mm-wide CFRP sheet at a distance of 130 mm along its length. These beams were compared with the un-strengthened beam (BN beam). In addition, a simply supported boundary with a clear span of 2300 mm was applied to the beams. The specimens were tested using a three-point loading with 4×10^{-4} m/s of loading rate. The loading rate was categorized as a static loading rate [33]. In addition, all material properties were tested at a static condition. The average value of concrete compressive strength (f_c') was 27.46 MPa. Furthermore, D10 and D16 of the reinforcement steel had a yield stress (f_y) of 350.67 and 492.25 MPa, respectively, and reached 500.85 and 727.51 MPa tensile strength (f_u) for D10 and D16, respectively. The mechanical properties of the CFRP rod were obtained from PT. SIKA Indonesia, which reported a modulus of elasticity of 148 GPa and a tensile strength of 3100 MPa.

Furthermore, a continuous study of a high loading rate (0.5 m/s) was conducted by Nugroho et al. [34]. The material and specimen geometry were the same as in the study by Haryanto et al. [20]. A strain gauge was attached to the reinforcement steel and concrete to record the strain response of the material and generate the strain rate.

2.2 Constitutive laws of models

2.2.1 Concrete

The analytical model formulated in Response-2000 considered the nonlinear properties of concrete under compression and the stress-strain relationships. Response-2000 provides a concrete model, formulated by Popovics [35] and slightly modified by Porasz [36], as expressed in Equations (1) to (3).

$$f_c = \left(\frac{\varepsilon_c}{\varepsilon_{co}}\right) f_c' \frac{n}{n-1+\left(\varepsilon_c/\varepsilon_{co}\right)^{nk}} \tag{1}$$

$$n = 0.8 + \frac{f_c'}{17} \tag{2}$$

$$k = \begin{cases} 1.0 & \text{if } \varepsilon_c/\varepsilon_{co} \le 1 \\ 0.67 + f_c'/62 & \text{if } \varepsilon_c/\varepsilon_{co} > 1 \end{cases} \tag{3}$$

In the given equation, f_c represents the concrete compressive stress (MPa) at a specific strain value (ε_c), f_c' represents the compressive strength of concrete (MPa), ε_{co} represents the strain at peak compressive strength, n represents the parameter for fitting the curve, and k represents the factor of loss in post-peak ductility for high-strength concrete.

Within this investigation, a modified Hognestad [37] stress-strain model was considered for comparative purposes, alongside the Popovics model. The modified Hognestad model is characterized by a non-linear curve for the ascending segment and a linear descent of stress-strain relationship for the descending segment, reaching a value of 0.15% of the compressive strength at ultimate strain (ε_{cu} = 0.0038). Equation (4) shows the ascending segment of the model.

$$f_c = f_c' \left[\frac{2\varepsilon_c}{\varepsilon_{co}} - \left(\frac{\varepsilon_c}{\varepsilon_{co}}\right)^2\right] \tag{4}$$

Furthermore, it is assumed that concrete in tension follows a linear behavior until the occurrence of initial cracking. The purposed cracking strength (f_{cr}) in Equation (5) is employed in Response-2000. It is appropriate for the structural analysis of a large volume of concrete and a better fit for higher strength data.

$$f_{cr} = 0.45\ f_c'^{\,0.4} \tag{5}$$

After cracking, the RC element retains the capacity to bear tension between these cracks through the action of bonding. The presence of concrete tension between cracks effectively results in a more substantial cross section than that of a bare bar, a phenomenon commonly referred to as 'tension stiffening'. In line with this theory, Response-2000 suggests the tension stiffening model proposed by Bentz [25], which accounts for the bond between the reinforcing bars and the concrete that causes concrete tension between the cracks, as detailed below:

$$f_1 = \frac{f_t}{1+\sqrt{3.6M\cdot\varepsilon_1}} \tag{6}$$

$$M = \frac{A_c}{\sum d_b \pi} \tag{7}$$

where f_1 is the principal average concrete tensile stress, ε_1 is the principal tensile strain, M is the bonding parameter (mm), A_c is the concrete area effectively bonded to the bar, and d_b is the diameter of the reinforcing bar in the concrete-stiffened area.

The concrete tensile strength (f_t) was estimated from concrete compressive strength data. Xu and Wen [38] proposed an equation for tensile strength, which has undergone calibration and validation through experiments using concrete materials with analogous compressive strengths, as documented in the literature, and is represented as follows:

$$f_t = 0.54\sqrt{f_c'} \tag{8}$$

Meanwhile, Japan Society of Civil Engineers (JSCE) [39] estimated tensile strength using Equation (9).

$$f_t = 0.23\left(f_c'\right)^{2/3} \tag{9}$$

2.2.2 Steel reinforcement and CFRP rod

The stress-strain relationship of steel reinforcement typically consists of three distinct phases: (1) the initial linear-elastic phase, (2) the yield plateau, and (3) the strain-hardening phase, which may exhibit linear or non-linear characteristics until rupture. The subsequent explanation of hysteresis behavior provides insight into the fundamental curve, as outlined by the models

proposed by Seckin [40] or Menegotto and Pinto [41], through the monotonic stress-strain curve. Meanwhile, the equation to calculate the steel reinforcement stress, f_s, for both tension and compression is as follows:

$$f_s = \begin{cases} E_s \varepsilon_s & \text{for} \quad \varepsilon_s < \varepsilon_y \\ f_y & \text{for} \quad \varepsilon_y < \varepsilon_s \le \varepsilon_{sh} \\ f_u + (f_y - f_u)\left(\dfrac{\varepsilon_u - \varepsilon_s}{\varepsilon_u - \varepsilon_{sh}}\right)^P & \text{for} \quad \varepsilon_{sh} < \varepsilon_s \le \varepsilon_u \\ 0 & \text{for} \quad \varepsilon_u < \varepsilon_s \end{cases} \tag{10}$$

where ε_s represents the strain ($\varepsilon_s = |\varepsilon_s|$), ε_y represents the yield strain, ε_{sh} represents the initial strain at the beginning of the strain hardening phase, ε_u represents the ultimate strain, E_s represents the elastic modulus, f_y represents the yield strength, f_u represents the ultimate strength, and P represents the strain-hardening parameter. It is noteworthy that the post-yield strain-hardening phase can exhibit either a linear (termed trilinear with P = 1) or nonlinear behavior (P = 4). Meanwhile, the strain hardening modulus, E_{sh}, is presented as follows:

$$E_{sh} = \left(\frac{f_u - f_y}{\varepsilon_u - \varepsilon_{sh}}\right) \tag{11}$$

In addition, a CFRP rod was provided by PT. SIKA Indonesia, with a product named 'Sika® CarboDur® BC8'. The CFRP rod does not exhibit any plastic behavior (yielding) before rupture or is characterized by a linearly elastic stress-strain relationship until failure with an average value of rupture strain. Therefore, this study assumed a perfectly elastic stress-strain curve for the CFRP rod material. As shown in the data sheet for the product, this type of CFRP rod has 148 GPa average elastic modulus, 3100 MPa average tensile strength, and rupture strain at 0.021.

2.3 Strain rate sensitivity of materials

2.3.1 Concrete

Structural concrete elements experience a dynamic response in high-strain-rate conditions, such as during intense impacts or seismic events. It has been shown that the strain-rate sensitivity of concrete material results in variations in its mechanical characteristics at different strain rates. The strain-rate sensitivity of concrete has been well explored in the literature [42-61]. Experimental evidence indicates that, under dynamic loading conditions, concrete can experience an enhancement in its failure stress, both in compression and tension. Recognizing the importance of these dynamic properties, several technical codes and researchers have contributed to their development to predict the real behavior of structures under high strain rates. These predictive formulations for dynamic compressive and tensile strength depend specifically on the strain rate values.

Fujikake et al. [62] employed the relationship function of strain rate (ε) to determine the dynamic properties of concrete. The dynamic compressive strength ($f_{cd}^{\cdot}$) is given in the dynamic increase factor (*DIF*) as follows [63]:

$$DIF_{fc} = \frac{f_{cd}^{\cdot}}{f_c^{\cdot}} = \left(\frac{\dot{\varepsilon}}{\dot{\varepsilon}_{sc}}\right)^{0.006\left[\log(\dot{\varepsilon}/\dot{\varepsilon}_{sc})\right]^{1.05}} \tag{12}$$

where $f_c^{\cdot}$ is the compressive strength under static loading (MPa) and $\dot{\varepsilon}_{sc}$ is the reference static strain rate, which is equal to 1.2×10^{-5} s^{-1}.

Meanwhile, the dynamic concrete tensile strength (f_{td}) adopted from Ross et al. [64], is as shown in Equation (13).

$$DIF_{ft} = \frac{f_{td}}{f_t} = \exp\left[0.00126\left(\log_{10}\frac{\dot{\varepsilon}}{\dot{\varepsilon}_{st}}\right)^{3.373}\right] \tag{13}$$

where $\dot{\varepsilon}_{st} = 1\times10^{-7}$ s^{-1} and f_t is the tensile strength under static loading (MPa) [40].

The European CEB code [65] recommended the following empirical formulation for the dynamic increase factor in compression and tension as follows:

$$DIF_{fc} = \frac{f_{cd}^{\cdot}}{f_c^{\cdot}} = \begin{cases} \left[\dfrac{\dot{\varepsilon}}{\dot{\varepsilon}_s}\right]^{1.026\delta} & \dot{\varepsilon} \le 30s^{-1} \\ \beta\left[\dfrac{\dot{\varepsilon}}{\dot{\varepsilon}_s}\right]^{1/3} & \dot{\varepsilon} > 30s^{-1} \end{cases} \tag{14}$$

$$DIF_{ft} = \frac{f_{td}}{f_t} = \begin{cases} \left[\dfrac{\dot{\varepsilon}}{\dot{\varepsilon}_{st}}\right]^{1.0168\lambda} & \dot{\varepsilon} \le 30s^{-1} \\ \alpha\left[\dfrac{\dot{\varepsilon}}{\dot{\varepsilon}_{st}}\right]^{1/3} & \dot{\varepsilon} > 30s^{-1} \end{cases} \tag{15}$$

where $\delta = \frac{1}{(5+9f_c/f_{co})}$, f_{co} = 10 MPa, $\beta = 10^{6.156\delta-2}$, $\dot{\varepsilon}_s$ = 30×10^{-6} s^{-1}, $\lambda = \frac{1}{(10+0.6f_c^{\cdot})}$, $\alpha = 10^{7.11\lambda-2.33}$, and $\dot{\varepsilon}_{st} = 3\times10^{-6}$ s^{-1}.

In 1998, Tedesco and Ross [55] conducted a comprehensive experimental program to obtain the effect of strain rate on the compressive and tensile strength of concrete. The outcomes were DIF regression equations, as presented in the following expressions:

$$DIF_{fc} = \frac{f_{cd}^{\cdot}}{f_c^{\cdot}} = \begin{cases} 0.00965\log\dot{\varepsilon} + 1.058 > 1 & \dot{\varepsilon} \le 63.1s^{-1} \\ 0.758\log\dot{\varepsilon} - 0.289 < 2.5 & \dot{\varepsilon} > 63.1s^{-1} \end{cases} \tag{16}$$

$$DIF_{ft} = \frac{f_{td}}{f_t} = \begin{cases} 1 + 0.1425\left[\log\dot{\varepsilon} + 5.856\right] > 1 & \dot{\varepsilon} \le 2.32\,s^{-1} \\ 1 + 2.929\left[\log\dot{\varepsilon} - 0.0635\right] \le 6 & \dot{\varepsilon} \le 2.32\,s^{-1} \end{cases} \tag{17}$$

Gebbeken and Greulich [66] devised a hyperbolic function to model the enhancement of tensile strength through strain rate effects, expressed as follows:

$$DIF_{ft} = \frac{f_{td}^{\cdot}}{f_t^{\cdot}} = \left\{\left[\tanh\left(\left(\log\left(\dot{\varepsilon}/\dot{\varepsilon}_0\right) - Wx\right)S\right)\right]\left[\frac{Fm}{Wy} - 1\right] + 1\right\}Wy \tag{18}$$

where Fm is a limit enhancement parameter, Wx, Wy, and S are shape parameters obtained by formula-fitting based on experimental results, and $\dot{\varepsilon}_0$ is a reference strain rate, $\dot{\varepsilon}_0$ = 1.0 s^{-1}. Notably, Xu and Wen [38] proposed specific

parameter values (Fm = 10, Wx = 1.6, S = 0.8, and Wy = 5.5), which exhibit remarkable concordance with the experimentally obtained DIF_{ft} for concrete materials. Furthermore, Xu and Wen [38] recommended a formulation of DIF_{fc} developed from DIF_{ft} and corrected for radial inertial effects, R_c [61], see Equations (19) and (20):

$$DIF_{fc} = \frac{f_t}{f_c'}\left(DIF_{ft} - 1\right) + R_c \tag{19}$$

$$R_c = \begin{cases} 1 + 0.03438\left(\log \dot{\varepsilon} + 3\right) & \dot{\varepsilon} < 10^2\, s^{-1} \\ 8.5303 - 7.1372 \log \dot{\varepsilon} + 1.729 \log^2 \dot{\varepsilon} & \dot{\varepsilon} > 10^2\, s^{-1} \end{cases} \tag{20}$$

Another famous empirical DIF_{ft} model was proposed by Malvar and Ross [67] and can be written as:

$$DIF_{ft} = \frac{f_{td}}{f_t} = \begin{cases} \left[\dfrac{\dot{\varepsilon}_d}{\dot{\varepsilon}_{ts}}\right]^{\delta} & \dot{\varepsilon}_d \le 1 s^{-1} \\ \beta\left[\dfrac{\dot{\varepsilon}_d}{\dot{\varepsilon}_{ts}}\right]^{1/3} & \dot{\varepsilon}_d > 1 s^{-1} \end{cases} \tag{21}$$

where $\delta = \dfrac{1}{\left(1+8\frac{f_c'}{f_{c0}'}\right)}$, f_{c0}' = 10 MPa, $\dot{\varepsilon}_{ts}$ = 10^{-6} s^{-1}, and β = $10^{6\delta-2}$.

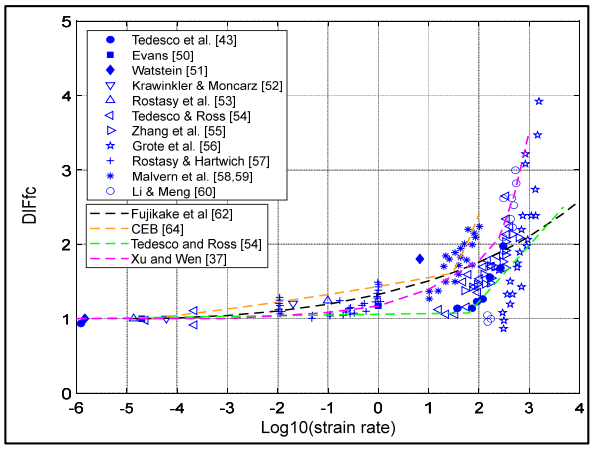

Fig. 2. Comparison of experimentally obtained compressive dynamic increase factor with empirical formulation used in the present study.

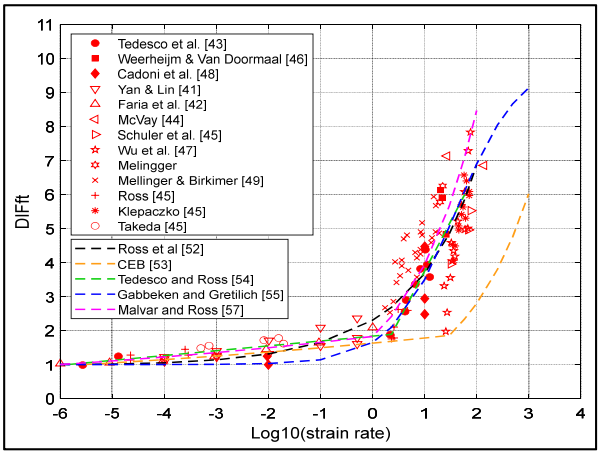

Fig. 3. Comparison of experimentally obtained tensile dynamic increase factors with empirical formulations used in the present study.

Figure 2 and Figure 3 compare the data from the literature for the dynamic increase factor for compression and tension with empirical formulations from several studies. It is shown that all empirical formulations represent the behavior of concrete under dynamic conditions. The DIF significantly increases when the strain rate is higher than ±1 s^{-1}.

2.3.2 Steel reinforcement and CFRP rod

In the case of reinforcement steel, akin to many other metallic materials, it is noteworthy that the dynamic mechanical behavior is significantly different from that under static load conditions. These phenomena, associated with steel strain-rate sensitivity, are related to the evolution of dynamic dislocations in its microstructure [68, 69]. As the strain rate increases, it is possible to observe the change of mechanical properties of reinforcing steel, notably an increase in both yield strength (f_y) and ultimate strength (f_u), followed by an increase in ultimate strain (ε_u) [68-73]. In contrast, there are no observed changes in relation to Young's modulus.

The following equation was proposed by the Japan Society of Civil Engineers [39] to determine the dynamic increase factor of yield stress (DIF_{fy}):

$$DIF_{fy} = \frac{f_{yd}}{f_{ys}} = \left(1.202 + 0.040' \log \dot{\varepsilon}\right)^3 \quad 1 \tag{22}$$

where f_{ys} and f_{yd} are the static and dynamic yield stress of reinforcement steel. The aforementioned equation is applicable for the analytical evaluation of RC beams under various strain rates and was employed in prior research by Fujikake et al. [62]

CEB Information Bulletin No. 187 [73] provides the following predictive formulation for the DIF, concerning the yielding stress of hot-rolled reinforcing steel:

$$DIF_{fy} = \frac{f_{yd}}{f_{ys}} = 1 + \frac{6.0}{f_{ys}} . \ln \frac{\dot{\varepsilon}}{\dot{\varepsilon}_0} \tag{23}$$

$$DIF_{fu} = \frac{f_{ud}}{f_{us}} = 1 + \frac{7.0}{f_{us}} . \ln \frac{\dot{\varepsilon}}{\dot{\varepsilon}_0} \tag{24}$$

where DIF_{fy} and DIF_{fu} are the dynamic increase factor for yield stress and ultimate tensile strength, respectively, f_{yd} and f_{ud} are the dynamic yield stress and dynamic ultimate tensile strength, while f_{ys} and f_{us} are the static yield stress and dynamic ultimate tensile strength, respectively, $\dot{\varepsilon}$ is considered to be the strain rate referring to the quasi-static strain rate ($\dot{\varepsilon}_0$), which is equal to $5' 10^{-5}$ s^{-1}.

In addition, Malvar [69] proposed the following expression, based on a comprehensive review of the research on the effect of strain rate on steel reinforcing bars:

$$DIF_{fy} = \frac{f_{yd}}{f_{ys}} = \left(\frac{\dot{\varepsilon}}{10^{-4}}\right)^{0.074 - 0.040\frac{f_{yd}}{414}} \tag{25}$$

$$DIF_{fu} = \frac{f_{ud}}{f_{us}} = \left(\frac{\dot{\varepsilon}}{10^{-4}}\right)^{0.019-0.009\frac{f_{yd}}{414}} \quad (26)$$

where f_{ys}, f_{yd}, f_{us}, and f_{ud} are required in MPa. These formulations are only applicable for strain rate in range from 10^{-4} to 10 s^{-1} and for $290 < f_{ys} < 710$ MPa.

On the other hand, the variations in strain rate had no effect on unidirectional CFRP rod properties. This agreement followed the established data from Gao et al. [74], where the tensile strength and Young's modulus of unidirectional CFRP (0° to load direction) under strain rate influence are hardly to be discovered.

3 Result and discussion

3.1 Validation model in static loading rate

The models were validated by conducting a comparison between the results from the Response-2000 model and the ultimate load from the experimental results under the static loading rate. Since there is no material testing data for concrete tensile strength, the tests compared two formulations for concrete tensile strength: Xu and Wen [38], indicated as '*ft1*', and JSCE [39], indicated as '*ft2*'. In addition, two types of reinforcing steel models were included. The first model to be discussed is the bilinear steel model, indicated as '*SM1*', which assumes that, after the yield point is reached, the stress remains constant and equal to the yield strength. Another model adopted the real stress-strain behavior expressed in Equation (10). This steel model is denoted as '*SM2*'. Meanwhile, the Popovics model [35] was evaluated for the concrete model. Table 1 shows the comparison between experimental and analytical models, in terms of ultimate load. Furthermore, the percentage differences between the experimental results for BN, BH, and BF are seen in Figure 4.

Table 1. Comparison results of ultimate load (kN) from experimental and analytical models.

Beam	Combination material model				Exp.
	ft1	*ft1*	*ft2*	*ft2*	
	SM1	*SM2*	*SM1*	*SM2*	
BN	154.6	162.0	154.6	162.0	158.36
BH	194.0	194.0	189.4	189.4	197.06
BF	203.4	203.4	200.0	200.0	217.89

Variations in the concrete tensile model did not give any significant results on the BN beam, while the bilinear steel model slightly reduced ultimate capacity. It is indicated that the beam failed after reaching the yield point of steel. In contrast, the steel model did not influence the ultimate load capacity, but lower tensile strength (ft2) provided a significant reduction in the strengthened beams. From this result, the best combination, which was ft1 and SM1, was taken into the next test using the concrete model for the Hognestad model [37]. Table 2 shows the comparison between the Hognestad and Popovics models. The Hognestad model improved the accuracy of Response-2000 by increasing the ultimate load because the model has a better descending branch after the peak, the slope being relatively higher compared to the Popovics model. The absolute average of all beams using the Hognestad and Popovics models were 2.88% and 3.53%, respectively. Therefore, this combination was proposed to predict the ultimate load under high loading rates.

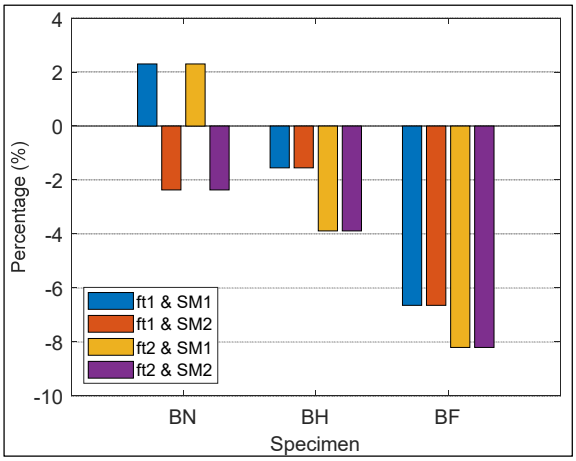

Fig. 4. Combination of tensile strength and steel model.

Table 2. Accuracy comparison between the Popovics and Hognestad models.

Specimen	Model	Difference
BN	Popovics	-2.37%
	Hognestad	-1.87%
BH	Popovics	-1.55%
	Hognestad	-0.94%
BF	Popovics	-6.65%
	Hognestad	-5.82%

3.2 Model under high loading rate

By using the equation for DIF-strain rate, the static material properties were converted into their dynamic properties based on material strain rates. In addition, the strain rate inside the beam was obtained from strain gauges. During the yielding phase of steel, the maximal strain rate at the middle span of longitudinal tensile steel was measured to be 0.428/s. Meanwhile, concrete strain was observed to be consistent with the strain rate prior to the occurrence of any cracking in the concrete. The average value of this strain rate was measured at 0.23/s.

Table 3. Testing combination for DIF concrete compressive and tensile strength.

Code	DIF_{fc} model	DIF_{ft} model
CT1	Fujikake et al. [62]	Ross et al. [63]
CT2	European CEB [64]	European CEB [64]
CT3	Tedesco and Ross [54]	Tedesco and Ross [54]
CT4	Gebbeken and Greulich [65]	Xu and Wen [37]
CT5	European CEB [64]	Malvar and Ross [66]

In this study, the combination of DIFfc and DIFft were considered, based on their use in previous research on RC under dynamic loads. Table 3 presents the combination of

the dynamic compressive strength model and the dynamic tensile strength model, as well as a representative combination code. Furthermore, the empirical formulations from the JSCE [39], Malvar [70], and CEB codes [71] were utilized for obtaining the yield strength of steel.

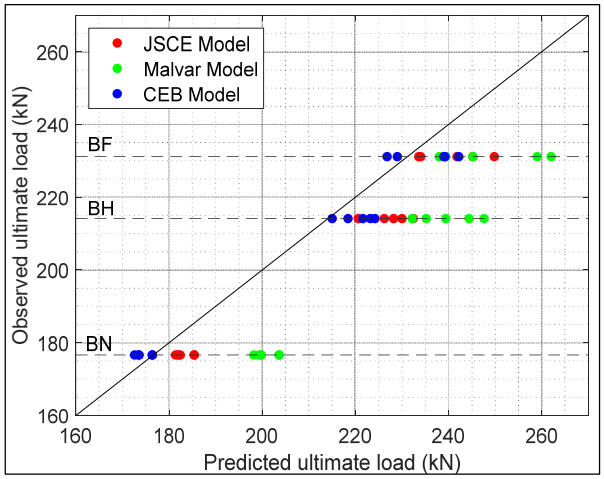

Fig. 5. Results of tested beam using several combinations of empirical formulations.

Figure 5 provides a summary of all the predictions. The Malvar model overestimated yield strength, resulting in higher predictions than the JSCE and CEB empirical formulations. The concrete's tensile strength did not significantly enhance the BN beam. In contrast, it had a significant impact on strengthened beams. Finally, the combination of *CT3* and *CT4* had better accuracy than other models, as presented in Table 4. Table 4 shows that the lowest absolute average was determined on the analytical model that adopted the CEB steel model and combination *CT4*.

Table 4. Result of combination *CT3* and *CT4* using JSCE and CEB steel models.

Specimen	JSCE steel model		CEB steel model	
	CT3	*CT4*	*CT3*	*CT4*
BN	2.70%	3.04%	-2.28%	-1.83%
BH	5.64%	3.02%	1.99%	0.41%
BF	1.06%	1.24%	-0.93%	-1.88%
Abs. Average	**3.13%**	**2.43%**	**1.73%**	**1.37%**

Using rate-dependent material behavior, Response-2000 is capable of providing accurate predictions that closely replicate experimental responses. Consequently, additional research could be conducted using Response-2000 for parametric studies, including the loading rate effect. However, insufficient research has been conducted to establish relationships between loading rates and strain rate values on material within an RC beam.

4 Conclusion

This study was conducted to assess the capability of Response-2000 to predict the flexural capacity of strengthened beams. The strengthened beams were designed by embedding CFRP rods on the tensile surface of the beam. The prediction limit depends only on the ultimate load. The test began by checking the validity of the concrete tensile strength model and the steel model by comparing them to experimental values under static loading rates. The material used had properties at a static rate. The results showed that the concrete tensile strength has a negligible effect on the BN beam, while for strengthened beams, the ultimate loads were influenced by the tensile strength of the concrete. The stress-strain concrete model from Hognestad could increase the ultimate load, resulting in better accuracy. This validation model was used for testing RC beams under high loading rates by converting the static properties of concrete (compressive and tensile strength) and reinforcing steel. Three empirical formulations of the yield strength of steel were tested. The findings showed that the Malvar model provided an overestimated effect on the ultimate load. Five combinations of compressive and tensile empirical formulations were tested for concrete. It can be concluded that concrete's tensile strength did not significantly enhance the BN beam. In contrast, it had a significant impact on strengthened beams. Combinations *CT3* and *CT4* were close to the observed ultimate load. Finally, good accuracy was obtained using the CEB steel model and *CT4* combination. The findings showed that the Response-2000 program can make quick predictions of flexural capacity as a preliminary design tool for strengthening RC beams.

The authors express their gratitude for the financial support they received from the Ministry of Science and Technology (MOST), Taiwan, under grant number MOST 110-2625-M-006-016, as well as the National Center for Research on Earthquake Engineering (NCREE), Taiwan. Furthermore, the provision of material support from PT. SIKA Indonesia is greatly valued.

References

1. Y. Haryanto, B.S. Gan, A. Maryoto, Int. J. Technol. **8**, 132 (2017)
2. Y. Haryanto, B.S. Gan, A. Widyaningrum, A. Maryoto, J. Teknol. **6**, 233 (2017)
3. Y. Haryanto, B.S. Gan, A. Widyaningrum, N.G. Wariyatno, A. Fadli, J. Teknol. **80**, 145 (2018)
4. Y. Haryanto, H.-T. Hu, A.L. Han, A.T. Atmajayanti, D.L.C. Galuh, B. A. Hidayat, J. Teknol. **81**, 145 (2019)
5. Y. Haryanto, A.L. Han, H.-T. Hu, F.-P. Hsiao, B.A. Hidayat, A. Widyaningrum, J. Chinese Inst. Eng. **44**, 193 (2021)
6. F.-P. Hsiao, P.-W. Weng, Y.-A. Li, T. Kawamoto, Y.-C. Lin, Y. Haryanto, Compos. Struct. **324,** 117562 (2023)
7. L. C. Bank, Composites for construction: structural design with FRP materials (John Wiley & Sons, New Jersey, 2006)
8. C.E. Bakis, L.C. Bank, V.L. Brown, E. Cosenza, J.F. Davalos, J.J. Lesko, A. Machida, S.H. Rizkalla, T.C. Triantafillou, J. Compos. Constr. **6**, 73 (2002)
9. J. G. Teng, J.-F. Chen, S. Smith, L. Lam, FRP-strengthened RC structures (John Wiley & Sons, New York, 2002)

10. Y. Haryanto, H.-T. Hu, A.L. Han, F.-P. Hsiao, C.-J. Teng, B.A. Hidayat, L. Nugroho, Period. Polytech. Civ. Eng. **65**, 878 (2021)
11. L. De Lorenzis, J.G. Teng, Compos. Part B Eng. **38**, 119 (2007)
12. R. Seracino, M.R. Raizal Saifulnaz, D.J. Oehlers, J. Compos. Constr. **11**, 62 (2007)
13. R. Seracino, N.M. Jones, M.S. M. Ali, M.W. Page, D.J. Oehlers, J. Compos. Constr. **11**, 401 (2007)
14. L. De Lorenzis, A. Nanni, J. Compos. Constr. **5**, 114 (2001)
15. J.A.O. Barros, A.S. Fortes, Cem. Concr. Compos. **27**, 471 (2005)
16. J.G. Teng, L. De Lorenzis, B. Wang, R. Li, T.N. Wong, L. Lam, J. Compos. Constr. **10**, 92 (2006)
17. Y. Haryanto, H.-T. Hu, A.L. Han, F.-P. Hsiao, C.-J. Teng, B.A. Hidayat, L. Nugroho, Comput. Concr. **28**, 347 (2021)
18. A.L. Han, H.-T. Hu, B.S. Gan, F.-P. Hsiao, Y. Haryanto, Arab. J. Sci. Eng. **47**, 12685 (2022)
19. Y. Haryanto, A.L. Han, H.-T.Hu, F.-P.Hsiao, B.S. Gan, L. Nugroho, C-C. Lin, , in Proceedings of the 33rd International Ocean and Polar Engineering Conference, ISOPE, 19–23 June 2023, Ottawa, Canada (2023)
20. Y. Haryanto, F.-P. Hsiao, H.-T. Hu, A.L. Han, A. Wiranata Chua, F. Salim, L. Nugroho, Compos. Struct. **301**, 116214 (2022)
21. S.S. Zhang, Y. Ke, E. Chen, H. Biscaia, W.G. Li, Compos. Struct. **279**, 114782 (2022)
22. I.A. Sharaky, L. Torres, J. Comas, C. Barris, Compos. Struct. **109**, 8 (2014)
23. ACI Committee 440: ACI 440.2R-17 (American Concrete Institute, Farmington Hills, USA, 2017)
24. ACI Committee 318, ACI 318-19 (American Concrete Institute, Farmington Hills, USA, 2019)
25. E.C. Bentz, Sectional analysis of reinforced concrete members (Ph.D. Thesis, University of Toronto, Toronto, Canada, 2000)
26. F.J. Vecchio, M.P. Collins, ACI J. **83**, 219 (1986)
27. I.M. Metwally, HBRC J. **8**, 99 (2012)
28. B. Suryanto, R. Morgan, A.L. Han, Civ. Eng. Dimens. **18**, 16 (2016)
29. F.J. Vecchio, W. Shim, J. Struct. Eng. **130**, 460 (2004)
30. Y. Haryanto, F.-P. Hsiao, H.-T. Hu, A.L. Han, B.A. Hidayat, L. Nugroho, in AIP Conference Proceedings of the 3rd International Conference on Engineering, Technology and Innovative Researches, ICETIR, 1 September 2021, Purbalingga, Indonesia (2023)
31. Y. Haryanto, H.-T. Hu, A.L. Han, F.-P. Hsiao, N.G. Wariyatno, B.A. Hidayat, J. Eng. Sci. Technol. **16**, 3295 (2021)
32. Y. Haryanto, H.-T. Hu, A.L. Han, F.-P. Hsiao, C.-J. Teng, B.A. Hidayat, N.G. Wariyatno, J. Chinese Inst. Eng. Trans. Chinese Inst. Eng. A **44**, 553 (2021)
33. S. Das Adhikary, B. Li, K. Fujikake, Int. J. Impact Eng. **47**, 24 (2012)
34. L. Nugroho, Y. Haryanto, H.-T. Hu, F.-P. Hsiao, A.L. Han, G. Pamudji, B.H. Setiadji, Compos. Struct. (to be published)
35. S. Popovics, Cem. Concr. Res. **3**, 583 (1973)
36. A. Porasz, An investigation of the stress-train characteristics of high strength concrete in shear (Ph.D. Thesis, University of Toronto, Toronto, Canada, 1989)
37. E. Hognestad. (Bulletin Series No. 399, Engineering Experiment Station, University of Illinois, Urbana, USA, 1951)
38. H. Xu, H. M. Wen, Int. J. Impact Eng. **60**, 76 (2013)
39. Japan Society of Civil Engineers, Standard specifications for concrete structures 2002, structural performance verification (JSCE, Tokyo, 2002) (in Japanese)
40. M. Seckin, Hysteretic behaviour of cast-in-place exterior beam-column sub-assemblies (Ph.D. Thesis, University of Toronto, Toronto, Canada, 1981)
41. M. Menegotto, P.E. Pinto, Method of analysis for cyclically loaded reinforced concrete plane frames including changes in geometry and non-elastic behavior of elements under combined normal force and bending, in Proceedings of the IABSE Symposium on Resistance and Ultimate Deformability of Structures Acted on by Well Defined Repeated Loads, Lisbon, Portugal (1973)
42. D. Yan, G. Lin, Cem. Concr. Res. **36**, 1371 (2006)
43. R. Faria, J. Oliver, M. Cervera, Int. J. Solids Struct. **35**, 1533 (1998)
44. J.W. Tedesco, J.C. Powell, C.A. Ross, M.L. Hughes, Comput. Struct. **64**, 1053 (1997)
45. M.K. McVay, Spall damage of concrete structures (Department of the Army Hattiesburg, MS, USA, 1988)
46. H. Schuler, C. Mayrhofer, K. Thoma, Int. J. Impact Eng. **32**, 1635 (2006)
47. J. Weerheijm, J.C.A.M. VanDoormaal, Int. J. Impact Eng. **34**, 609 (2007)
48. H. Wu, Q. Zhang, F. Huang, Q. Jin, Int. J. Impact Eng. **32**, 605 (2005)
49. E. Cadoni, K. Labibes, M. Berra, M. Giangrasso, C. Albertini, Mag. Concr. Res. **52**, 365 (2000)
50. F.M. Mellinger, D.L. Birkimer, (Technical Report 4-46. U.S. Army Corps of Engineers, Ohio River Division Laboratories, Cincinnati, Ohio, 1966)
51. R.H. Evans, J. Inst. Civ. Eng. **18**, 296 (1942)
52. D. Watstein, J. Proc. **49**, 729 (1953)
53. H. Krawinkler, P.D. Moncarz, Spec. Publ. **73**, 1 (1982)
54. F.S. Rostasy, J. Scheuermann, K.H. Sprenger, Betonwerk+Fertigteil-Technik. **50**, 393 (1984)
55. J.W. Tedesco, C.A. Ross, J. Press. Vessel Technol. Trans. ASME **120**, 398 (1998)
56. M. Zhang, H.J. Wu, Q.M. Li, F.L. Huang, Int. J. Impact Eng. **36**, 1327 (2009)
57. D.L. Grote, S.W. Park, M. Zhou, Int. J. Impact Eng. **25**, 869 (2001)
58. F.S. Rostasy, K. Hartwich, Int. J. Cem. Compos. Light. Concr. **7**, 21 (1985)
59. L.E. Malvern, C.A. Ross, Dynamic response of concrete and concrete structures (Second Annual Technical Report, AFOSR contract no. F49620-83-K007, 1986)
60. L.E. Malvern, D.A. Jenkins, T. Tang, C.A. Ross, Dynamic compressive testing of concrete, in

Proceedings of the 2nd Symposium on the Interaction of Non-Nuclear Munitions with Structures, 15-18 April 1985, Panama City Beach, Florida (1985)
61. Q.M. Li, H. Meng, Int. J. Solids Struct. **40**, 343 (2003)
62. K. Fujikake, B. Li, S. Soeun, J. Struct. Eng. **135**, 938 (2009)
63. K. Fujikake, K. Mori, K. Uebayashi, T. Ohno, J. Mizuno, Constitutive model for concrete materials with high-rates of loading under tri-axial compressive stress states, in Proceedings of the 3rd International Conference on Concrete under Severe Conditions, JSCE, Tokyo (2001)
64. C.A. Ross, J.W. Tedesco, Mater. J. **86**, 475 (1989)
65. Comité Euro-International du Béton, CEB-FIP Model code 1990: Design code (Thomas Telford Publishing, 1993)
66. N. Gebbeken, S.Greulich, A new material model for SFRC under high dynamic loadings, in Proceedings of the 11th International Symposium Interaction of the Effects of Munitions with Sructures, ISIEMS, 5 May 2003, Mannheim, Germany (2003)
67. L.J. Malvar, C.A. Ross, ACI Mater. J. **95**, 735 (1998)
68. A. Uenishi, C. Teodosiu, Int. J. Plast. **20**, 915 (2004)
69. R.J. Mainstone, Matériaux Constr. **8**, 102 (1975)
70. L.J. Malvar, Mater. J. **95**, 609 (1998)
71. F. Lin, Y. Dong, X. Kuang, L. Lu, Mater. **9**, (2016)
72. D. Asprone, E. Cadoni, A. Prota, ACI Struct. J. **106**, 523 (2009)
73. Comité Euro-International du Béton, Concrete Structures under impact and impulsive loading: CEB Bulletin 187 (Lausanne, Switzerland, 1988)
74. D. Gao, Z. Bao, W. Han, X. Wang, S. Huang, L. Huang, Q. Chen, H. Zhao, Y. Xu, Polymers **15**, 2711 (2023)